WARWICK
THE UNIVERSITY OF WARWICK

Manuscript version: Author's Accepted Manuscript
The version presented in WRAP is the author's accepted manuscript and may differ from the published version or Version of Record.

Persistent WRAP URL:
http://wrap.warwick.ac.uk/167906

How to cite:
Please refer to published version for the most recent bibliographic citation information. If a published version is known of, the repository item page linked to above, will contain details on accessing it.

Copyright and reuse:
The Warwick Research Archive Portal (WRAP) makes this work by researchers of the University of Warwick available open access under the following conditions.

© 2022, Elsevier. Licensed under the Creative Commons Attribution-NonCommercial-NoDerivatives 4.0 International http://creativecommons.org/licenses/by-nc-nd/4.0/.

Publisher's statement:
Please refer to the repository item page, publisher's statement section, for further information.

For more information, please contact the WRAP Team at: wrap@warwick.ac.uk.

warwick.ac.uk/lib-publications

Remote Epitaxy of $In_xGa_{1-x}As$ (001) on Graphene Covered GaAs(001) Substrates

T. Henksmeier[1*], J.F. Schulz[2], E. Kluth[2], M. Feneberg[2], R. Goldhahn[2], A. M. Sanchez[3], M. Voigt[4], G. Grundmeier[4], D. Reuter[1]

[1]*Paderborn University, Department of Physics, Warburger Str. 100, 33089 Paderborn, Germany*
[2]*Otto von Guericke University Magdeburg, Institute of Physics, Universitätsplatz 2, 39106 Magdeburg, Germany*
[3]*Warwick University, Department of Physics, Coventry, CV4 7AL, UK*
[4]*Paderborn University, Department of Chemistry, Warburger Str. 100, 33089 Paderborn, Germany*

*Corresponding author: *tobias.henksmeier@upb.de*

ABSTRACT The heteroepitaxial growth of lattice mismatched layers is crucial for modern semiconductor device fabrication, but it is a significant challenge in epitaxy. Growth of lattice mismatched materials creates strain in the epitaxial layer, which is usually relaxed by introducing crystal defects deteriorating the device performance. Remote epitaxy on graphene covered substrates was recently proposed to offer a different relaxation pathway for the strained films. Here, we report on the remote heteroepitaxy growth by molecular beam epitaxy of $In_xGa_{1-x}As$-layers ($0<x\leq0.5$) on transfer graphene covered GaAs-(001) substrates. We show that a carefully optimized plasma treatment followed by UHV annealing allows $In_xGa_{1-x}As$ remote epitaxy on transfer graphene covered GaAs substrates. Detailed investigations on the strain relaxation of 200 nm thick $In_xGa_{1-x}As$-layers on graphene coved GaAs and for comparison on bare GaAs are presented. High-resolution X-ray-diffraction (HRXRD) and transmission electron microscopy (TEM) measurements reveal single crystalline growth on large areas. On bare GaAs we observe the well-known tilt of the $In_xGa_{1-x}As$ layers whereas on graphene no tilt is observed. The layers grown on graphene are more relaxed than layers grown on bare GaAs and their strain relaxation is symmetric whereas on bare GaAs the strain relaxation is stronger along the [110] direction.

Keywords: A3. Remote epitaxy ; A3. Molecular beam epitaxy ; B1. Graphene ; B2. Semiconducting III-V materials ; B2. Semiconducting gallium arsenide ;

1. Introduction

In semiconductor epitaxy, the integration of different materials has always been of great interest to combine their individual intrinsic electronic and optical properties to create new device functionalities. However, heteroepitaxy suffers from the lattice mismatch of different semiconductors, especially between film and substrate, which causes strain in the film. Above a critical thickness, this strain is plastically relaxed by the formation of dislocations in the epitaxial film deteriorating the optical and electrical performance. Thick metamorphic buffers with various grading schemes have been employed to reduce the dislocation density in the active region of a layer stack [1-3]. In contrast, nearly complete decoupling of layer and film is achieved in van-der-Waals epitaxy [4-8]. However, successful growth of III-As van-der-Waals semiconductors like GaAs was not possible so far due to the low substrate surface

potential [4-5]. The wettability of the surface and the missing crystal stability without an interacting substrate caused problems [4-5]. Recently, remote epitaxy was proposed as a promising approach to weaken the substrate-layer binding but still transferring the crystal orientation to the growing layer [8-14]. A monolayer graphene placed on the substrate introduces a substrate-layer-interaction gap. Layers grown on this graphene covered surface can be peeled off allowing the fabrication of free-standing semiconductor films and substrate reuse [9-16]. In the more delicate way of remote heteroepitaxy, a layer slip on the graphene as an alternative strain-relaxation mechanism besides dislocation introduction was observed [9,14]. Exceeding a critical strain energy, the layer starts to relax by slipping over the graphene surface instead of forming dislocations [14]. So far, remote epitaxy by MOCVD of several semiconductor material combinations was demonstrated, e. g., GaAs on GaAs [10-12], GaN on GaN or on SiC [9-12], InGaP and GaP on GaAs [14]. Often a dry transfer method was used to transfer monolayer graphene to the substrates rather than the simpler wet transfer method. It was shown that during wet transfer, the freshly oxide striped GaAs substrate re-oxidizes and thus prevents remote epitaxy [10]. However, commercially available CVD transfer graphene is arguably the simplest way to cover large substrate areas, even entire wafers, with graphene.

In this work, we present a study of remote heteroepitaxy by solid source molecular beam epitaxy of $In_xGa_{1-x}As$-layers ($0<x\leq 0.5$) on CVD-monolayer-graphene covered GaAs-(001) substrates. We focused this study to $x<0.5$, because this is the technological important composition range for realizing devices for the optical C-band. We also prepared a few selected $In_xGa_{1-x}As$ films with $x>0.5$, but we observed a strong degradation of the surface quality for growth on graphene covered substrates and decided not to investigate this composition range systematically. We present a plasma assisted preparation method to remove surface oxides of the GaAs after graphene transfer. X-ray photoelectron spectroscopy (XPS) and Raman spectroscopy reveal a graphene covered surface and an oxide free GaAs-graphene interface. We investigate the $In_xGa_{1-x}As$ nucleation on the graphene covered GaAs and performed two-step growth of 200 nm thick $In_xGa_{1-x}As$ layers. Detailed investigations of the $In_xGa_{1-x}As$-layers strain relaxation are performed and for comparison also of reference layers grown on bare GaAs. To gain detailed insight in the strain relaxation process, we performed reciprocal space mapping (RSM) and Raman-spectroscopy of all samples.

2. Experimental Details

All samples were prepared on 3” semi-insulating GaAs(001) quarter wafers. Monolayer graphene is transferred onto the wafers by a wet transfer technique. First, the GaAs wafers were dipped for 1 min in 10 % HCl solution and rinsed by DI-water to remove the native surface oxide layer. In parallel, small monolayer transfer graphene pieces (trivial transfer graphene from ACS materials) of around 4x4 mm stabilized by PMMA were released onto deionized water. Then, the PMMA-graphene stack is scooped by the freshly etched GaAs substrate without taking special care of the rotational orientation and dried for around 20 min at room temperature followed by a 30 min bake at 100 °C to increase the adhesion between the graphene layer and the GaAs substrate. The PMMA is then removed by an acetone bath at 50 °C for around 20 min. Finally, the sample is rinsed with IPA and DI-water and dried at 100 °C.

We found that this cleaning procedure was not enough to allow remote epitaxy in agreement with reports that solvents are not able to clean graphene completely from strongly adhering PMMA chains [17,18]. Thus, we performed an additional plasma cleaning step employing an ICP-reactive ion etching (RIE) system (PlasmaLab 100 from Oxford Instruments) comparable to other reports [17-19]. A 20 s short Argon-Hydrogen-plasma (5 sccm Ar and 10 sccm H) treatment was performed employing the following

parameters: chamber pressure = 42.5 Torr, ICP plasma power = 100 W, additional RF signal to the sample platen = 5 W.

The GaAs-graphene system was analyzed by XPS, Raman spectroscopy and atomic force microscopy (AFM). XPS was performed by means of an Omicron ESCA+ system at a base pressure of $<1\times10^{-8}$ Pa. An XM1000 source with monochromatic Al Kα-radiation (1486.7 eV) was used. The angle between source and analyzer was 102 °. The take-off angle with respect to the surface plane was 60 °. Measurements were performed without neutralization at a constant pass energy of 100 eV for survey and 20 eV for element spectra. Data evaluation was performed using CasaXPS Version 2.3.23PR1.0. Raman spectra were recorded by using a TriVista777 (S&I GmbH) equipped with a 532 nm laser source within a Raman microscope.

For overgrowth, the samples were then introduced into a III-V solid source MBE system (Dr. Eberl MBE Komponenten GmbH), where they were first baked 1 h at 200 °C in ultra-high vacuum and then transferred into the growth chamber. The samples were annealed for 5 min at 615 °C under As_4 overpressure to desorb any adsorbance, especially attached hydrogen atoms from the plasma treatment from the graphene. In addition, the non-graphene-covered GaAs substrate area is deoxidized. Then, the sample temperature was ramped to 425 °C. At this temperature the GaAs surface is stable without As_4 overpressure. The arsenic flux was stopped. The sticking coefficient of As on GaAs surface was reported to be zero for surface temperatures above around 300 °C. For graphene covered GaAs, we observed a similar behavior. Keeping the temperature above 300 °C ensures that there is no As-layer on the sample. The temperature was ramped to the nucleation temperature T_{nuk}. In [11,12] it was recommended to start the growth of GaAs on graphene covered GaAs with a monolayer of Ga. We follow this approach but instead of Ga we deposited a monolayer $\mathrm{In_xGa_{1-x}}$ with a rate of 1 $\mathrm{Ås^{-1}}$ first. Then, the As-flux is started (p_{As} = 0.9×10^{-5} mbar) while keeping the Ga and In shutter opened to form an $\mathrm{In_xGa_{1-x}As}$ nucleation layer. The deposition time was varied from 5 s to 50 s and different T_{nuk}. (300 °C, 385 °C, 485 °C) were tested. The material deposition was stopped, and the samples were analyzed by SEM.

The growth of 200 nm thick $\mathrm{In_xGa_{1-x}As}$ layers was done by a two-step process as proposed by [11]. We chose a thickness of 200 nm, because this thickness exceeds the critical layer thickness for growth on GaAs calculated by the model of People and Bean [20] over the tested indium concentrations range ($0.12\leq x<0.5$), so we are able to compare the film relaxation behavior for growth on graphene covered GaAs substrates and on bare GaAs. First, a nucleation layer was grown as described above. We choose 5 s material deposition at 300 °C. Then, the temperature was raised under As_4 overpressure to 385 °C and the nucleation layer was overgrown. After growth, ex-situ scanning electron microscopy (SEM) was used to investigate the surface quality of both, the overgrown graphene covered GaAs part, and the overgrown bare GaAs substrate. The graphene covered area was cleaved from the wafer and high-resolution X-ray diffraction measurements (HRXRD) were performed. Reciprocal space maps of the (-2-24) and (004) reflex were taken. The $\mathrm{In_xGa_{1-x}As}$ layer tilt was derived from the symmetric scan, while the $\mathrm{In_xGa_{1-x}As}$ layer indium content and the degree of relaxation was determined by evaluation of the (-2-24) reciprocal space map. Raman spectroscopy on the $\mathrm{In_xGa_{1-x}As}$ layers was investigated as a complementary method. Transmission electron microscopy (TEM) was performed on a selected sample to get insight on an atomic scale.

3. Results and Discussion

In Fig. 1, XPS spectra, Raman spectra and AFM images of the GaAs-graphene stack are summarized. a), c), e) show data obtained after the PMMA was removed from the graphene by the acetone bath as described above. In Fig. 1 a) the As-related XPS spectrum is shown. Two intense peaks around 41 eV related to the bond As atom electrons and a broader peak around 44.5 eV, which is related to As_2O_3 species, can be observed. Similar behavior was also observed in [10] and proof the re-oxidation of the GaAs substrate during the wet transfer of the graphene. Remote epitaxy is not possible on such layers. In contrast, after the short Ar+H-plasma treatment and annealing in UHV the oxide related peak vanishes, indicating an oxide free GaAs-graphene interface. Note, that the GaAs surface is protected also from reoxidation by the graphene during transfer between the machines. It has been reported that too harsh plasma processes might damage a graphene layer, but this would cause the GaAs reoxidation during sample transfer. It is astonishing that the oxide layer can apparently be removed by the H-plasma through the graphene layer and the exact mechanism how this works is not clear at the moment. We speculate that the hydrogen and the reaction product tunnel through the graphene or escape from the interface by pinholes in the graphene after moving laterally beneath the graphene. Further, we investigate the carbon related XPS spectra before and after plasma treatment and UHV annealing in Fig. 1 c)-d). Barely any difference is observed. However, the graphene surface AFM images clearly reveal an improved surface morphology. The root-mean-square roughness improves from 1.6 nm before to 0.4 nm after plasma treatment and UHV annealing. The corresponding Raman spectra of the graphene layer are shown in Fig. 1 e) and f). After plasma treatment and UHV annealing f) only a small defect related D peak appears but the 2D to G ratio change indicates some change on the graphene lattice. A similar spectrum was observed after plasma cleaning in [17]. There it was shown, that such a spectrum belongs to mostly intact monolayer graphene. We conclude from the XPS, Raman, and AFM measurements that the graphene layer is mostly still intact and only slightly damaged by the plasma treatment. With this preparation method, remote epitaxy is feasible as we discuss it in the following.

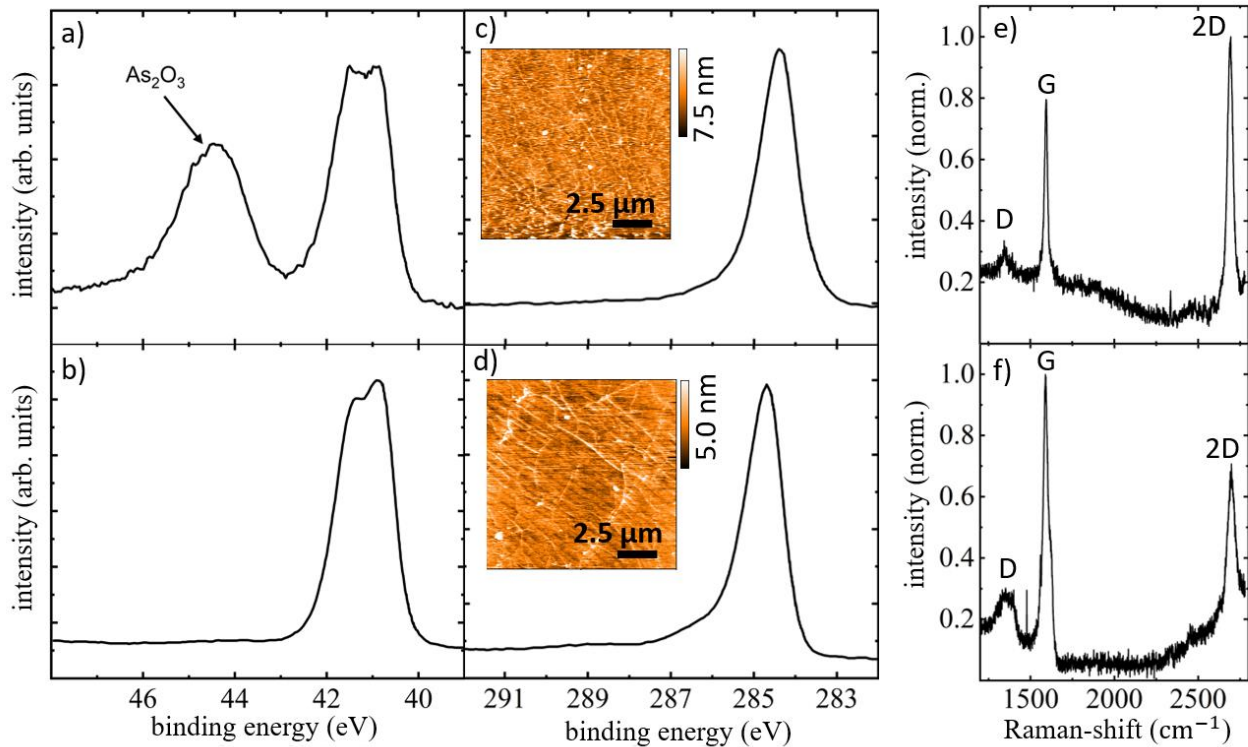

Figure 1*:* XPS, AFM and Raman measurement of the graphene-GaAs surface after acetone bath a), c), e) and after Ar+H-plasma treatment and UHV annealing b), d), f). A distinct As_2O_3 peak is observed in a) indication the substrate re-oxidation during the graphene transfer process.

In this paragraph, we want to discuss the $In_xGa_{1-x}As$ layer nucleation. In Fig. 2, SEM images of selected samples are shown. First note, that in all cases small islands are formed. This is in contrast to the usual layer-by-layer growth we observed for $In_xGa_{1-x}As$ growth on GaAs below the critical layer thickness (not shown here). This reveals a reduced influence on the GaAs substrate and the low surface energy of the graphene surface. This is consistent with the conclusions from Raman and XPS measurements, that the graphene layer is mostly intact. Fig. 2 a) shows the sample surface after depositing $In_{0.15}Ga_{0.85}As$ for 5 s at 300 °C. This equals a nominal coverage of 0.5 nm. Several small nuclei are distributed randomly over the surface. Increasing the deposition time to 50 s (=5 nm nominal coverage) results in larger nuclei covering the entire surface homogeneously, as show in Fig. 2 b). One clearly sees the boundaries, where the nuclei are coalesced. Fig. 2 c) shows the case of 50 s $In_{0.75}Ga_{0.25}As$ deposition at 300 °C. The layer is not fully closed, and the individual nuclei size differs more in contrast to the $In_{0.15}Ga_{0.85}As$ nuclei in a). For $In_{0.15}Ga_{0.85}As$ deposition at 485 °C some large nuclei are formed and only part of the graphene surface is covered (see Fig 2 d)). In summary, higher indium fraction and/or a higher surface temperature result in larger nuclei and more inhomogeneous surface coverage. The reason might be the Arrhenius like temperature dependence of the adatom mobility. At higher temperature, the adatoms exhibit a larger diffusion length and thus larger islands can be formed. A higher indium content also means a higher overall adatom mobility, because indium atoms exhibit a larger diffusion length compared to the Ga atoms, and thus favor the growth of larger nuclei.

We also checked the temperature stability of the $In_xGa_{1-x}As$ nuclei by increasing the substrate temperature under constant arsenic flux to up to 485 °C after nucleation. Then we ramped the temperature back to 300 °C and investigated the sample surface: Barely any change was observed neither

in size nor in surface coverage. The nuclei are stable at higher temperature during this temperature ramping step as the substrate-graphene-layer interaction is strong enough to stabilise them and ripening seems to be negligible.

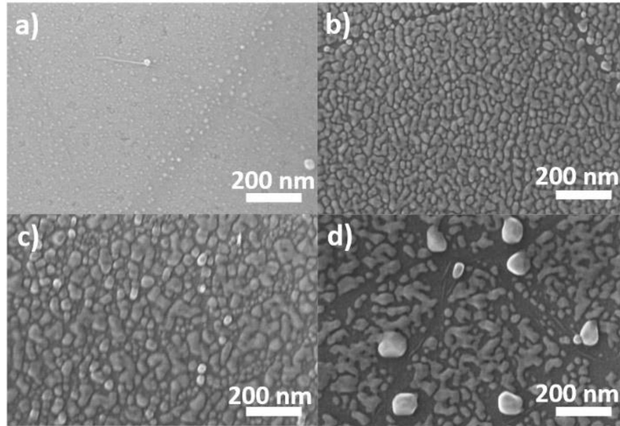

Figure 2: SEM images of several $\mathrm{In_xGa_{1-x}As}$ nucleation layer grown on graphene covered GaAs at different temperatures and indium concentrations: a) $\mathrm{T = 300\ °C,\ 15\ \%\ In,\ t_{dep} = 5\ s.}$ b) $\mathrm{T = 300\ °C,\ 15\ \%\ In,\ t_{dep} = 50\ s.}$ c) $\mathrm{T = 300\ °C,\ 75\ \%\ In,\ t_{dep} = 50\ s.}$ d) $\mathrm{T = 485\ °C,\ 15\ \%\ In,\ t_{dep} = 50\ s.}$ Note, that subsequent overgrowth of thicker films was performed on nucleation layers as shown in a) and b).

After the nucleation behaviour, we will now discuss the growth of 200 nm thick $\mathrm{In_xGa_{1-x}As}$ films with various indium concentrations. Omega-2theta scans (see Fig. S1) reveal the growth of single crystalline films oriented in the (001) direction. The substrate crystal orientation is transferred through the graphene to the $\mathrm{In_xGa_{1-x}As}$ film proving successful remote epitaxy. To gain deeper insight of the $\mathrm{In_xGa_{1-x}As}$ strain relaxation, reciprocal space maps (RSMs) around the symmetric (004) and the asymmetric (-2-24) reflex were taken. Fig. 3 shows exemplarily the RSMs of a 200 nm thick $\mathrm{In_{0.12}Ga_{0.88}As}$ layer grown on monolayer graphene and for comparison on bare GaAs. We measured RSMs with the incident plane either including the [110] or the [-110] direction, i.e., it was measured in four sample orientations differing by 90 °. While the on graphene grown $\mathrm{In_{0.12}Ga_{0.88}As}$ film in Fig. 3 a) exhibits a symmetric intensity distribution around the symmetry axes, the film grown on bare GaAs exhibits a considerable layer tilt d toward the <-110> direction; see arrow in Fig. 3 b). Layer tilt is well known within the GaAs/ $\mathrm{In_xGa_{1-x}As}$ system and was for example observed in thick $\mathrm{In_xGa_{1-x}As}$ buffer layers [2]. Due to the different crystal slip planes e.g., the (111) and (-1-1-1) plane the relaxation of a mismatched layer is not homogeneous [22] and a dominant relaxation in [110] direction occurs. Obviously, this is not the case for growth on graphene, which points to a different strain relaxation behaviour for growth on graphene. We derive the degree of film relaxation exemplarily from the asymmetric RSMs measured along the [-110] direction shown in Fig. 3 c) and d). The dashed lines indicate the relaxation triangle. An $\mathrm{In_{0.12}Ga_{0.88}As}$ film relaxation of around 60 % is observed for growth on the graphene. In contrast, the reference $\mathrm{In_{0.12}Ga_{0.88}As}$ film grown on bare GaAs is only relaxed around 10 %. The intensity distribution is broader for the film grown on graphene indicating more defects in this film compared to the reference sample. The defect density n_d is related to the FWHM of the (004)-rocking curve by $9b^2n_d = FWHM^2$; b is the dislocation Burger's vector modulus [22]. A measured high FWHM reveals a high dislocation density in the film. The $\mathrm{In_{0.12}Ga_{0.88}As}$ film grown on graphene (Fig 3. a)) exhibits a dislocation density of $\mathrm{n_d = 10 \times 10^9 cm^{-2}}$. In comparison, the reference film grown on bare GaAs shows $\mathrm{n_d = 10 \times 10^8 cm^{-2}}$, around a magnitude smaller. In conclusion, on graphene a higher dislocation density is observed, and the film is degraded.

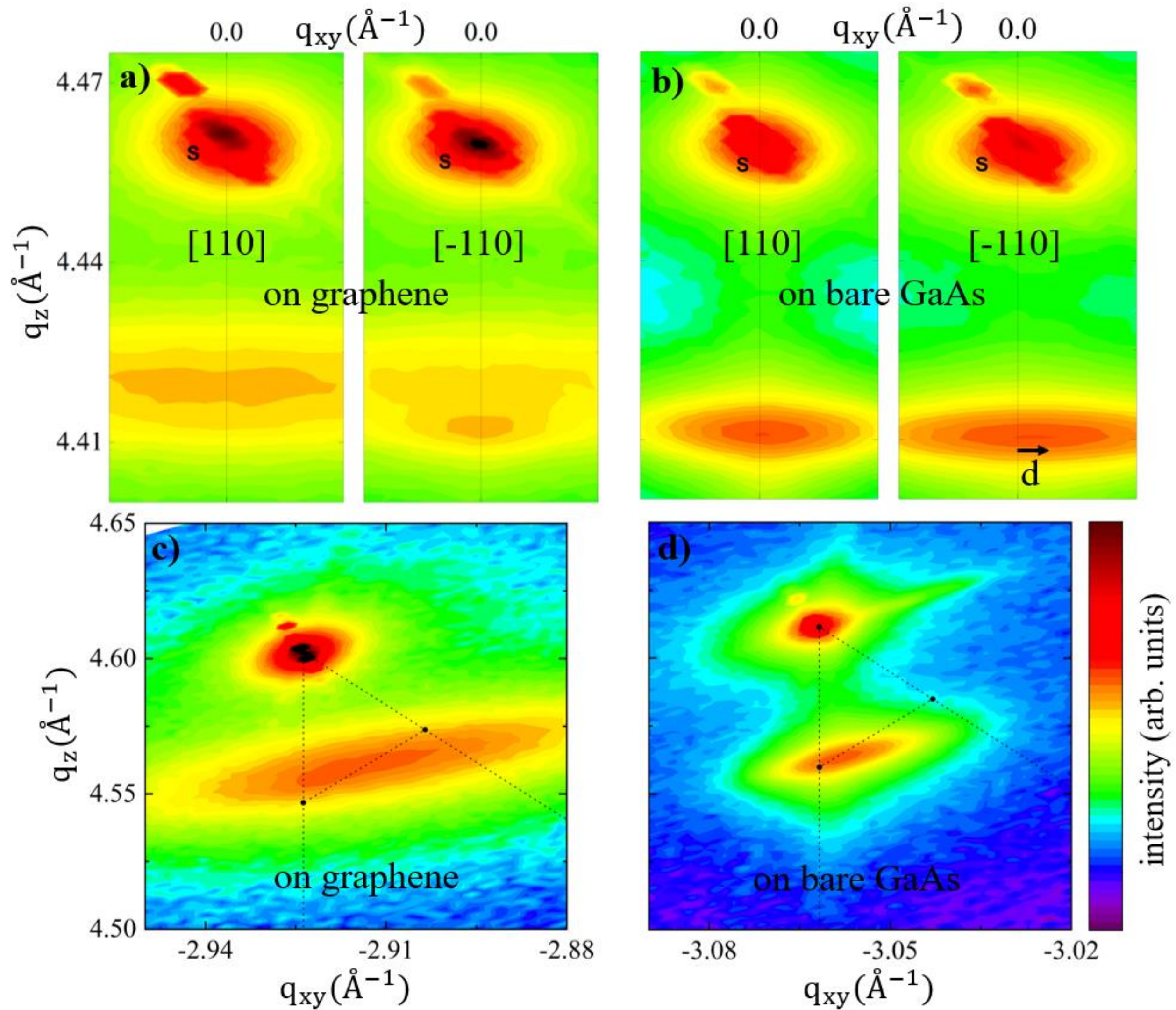

Figure 3*:* a)-b) Reciprocal space maps (RSMs) of the (004) reflex measured along both high-symmetry directions, [110] and [-110] and c)-d) of the (-2-24) reflex of a 200 nm thick $In_{0.12}Ga_{0.88}As$. A layer tilt d indicated by the arrow in b) is observed for the layer grown on bare GaAs (label S for substrate). A stronger relaxation of the $In_{0.12}Ga_{0.88}As$ film is observed on the graphene. A quantitative analysis reveals a larger $In_{0.12}Ga_{0.88}As$ peak FWHM of the film grown on graphene pointing to a larger defect density.

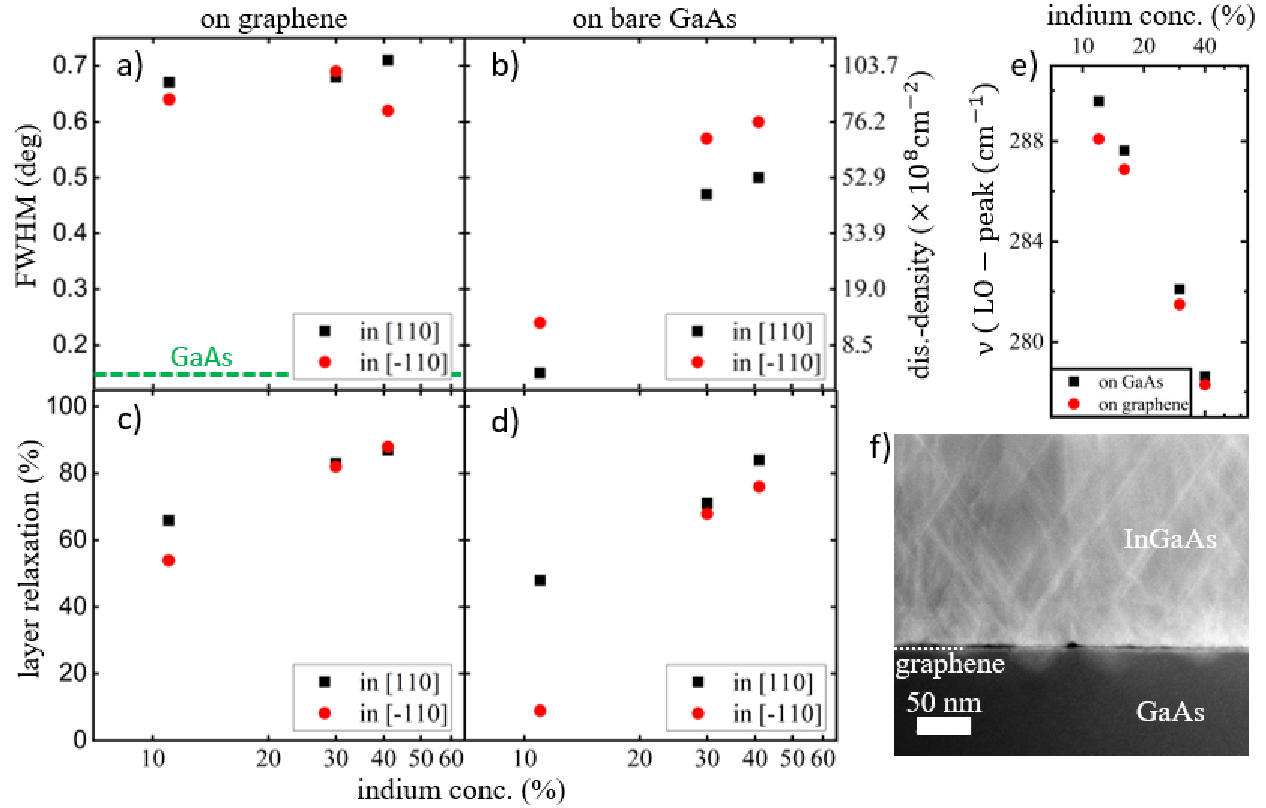

Figure 4: a)-d) $In_xGa_{1-x}As$ layer relaxation, HRXRD rocking curve FWHM and corresponding dislocation densities for 200 nm thick $In_xGa_{1-x}As$ films with various indium concentrations (0.12≤x<0.5) and for homoepitaxial growth of GaAs on graphene covered GaAs substrates for comparison (green dashed line). For GaAs growth on bare GaAs substrates, the FWHM is the same as for the substrate itself (0.007 deg). e) GaAs-LO wave-number of 200 nm thick $In_xGa_{1-x}As$ films plotted as a function of the indium concentration (0.12≤x<0.5). f) Dark-field TEM image of $In_{0.17}Ga_{0.83}As$ on graphene covered GaAs revealing a highly defective film.

We investigated this more quantitatively and performed growth of several 200 nm thick $In_xGa_{1-x}As$ films with various indium concentrations ($0.12 \leq x < 0.5$). In Fig. 4, the degree of layer relaxation and the rocking curve FWHM as well as the corresponding dislocation density are summarized for 200 nm thick $In_xGa_{1-x}As$ films with various indium concentrations ($0.12 \leq x < 0.5$). Data for both high symmetry directions, i.e., the [110] and the [-110] direction, are presented. The $In_xGa_{1-x}As$ layers grown on graphene exhibit a larger layer relaxation compared to growth on bare GaAs (Fig. 4 c) and d)), especially for low indium concentrations whereas the difference for x=0.5 becomes rather small. The degree of relaxation increases with and without graphene with increasing indium concentration. This is in accordance with the decrease of the critical layer thickness for larger lattice mismatch, as a larger strain energy builds up which is released by forming dislocations. The films relax stronger in [110] than in [-110] direction, where differences between the two directions are larger for growth on bare GaAs than for growth on graphene, especially for low indium fractions, whereas it almost vanishes for x > 0.3. These observations indicate a different strain relaxation mechanism on the graphene covered GaAs, which provides a lower activation energy. These results are confirmed by Raman spectroscopy measurements

summarized in Fig. 4 e) where the GaAs-LO wave-number ν is plotted as a function of the indium concentration. For the films on bare GaAs ν is larger indicating less relaxation in the films. The layers grown on graphene exhibit a larger relaxation over the entire indium concentration range but the difference to the films on bare GaAs is largest for low indium concentrations. We conclude that there is a strain relaxation mechanism with a lower activation energy compared to the formation of defects, which results to a more pronounced relaxation on graphene. Fig. 4 a) and b) show the dislocation densities calculated from the FWHM values obtained from the $In_xGa_{1-x}As$ rocking curves. $In_xGa_{1-x}As$ films grown on graphene exhibit a nearly constant dislocation density of around $n_d = 10 \times 10^9 cm^{-2}$ which seems to be independent on the indium content in the layer. In contrast, Fig. 4 b) shows that the dislocation density for growth on bare GaAs increases with increasing In-content: larger indium concentration and thus larger mismatch causes higher dislocation density as expected from standard theory [14,20]. To get information on the film's mosaicity, we performed additional HRXRD measurements of the asymmetric (-2-24)-reciprocal lattice reflex (not shown here) and analyzed the reciprocal lattice ellipse rotation qualitatively following the approach from R. Chierchia and co-workers [23]. For the growth on graphene covered GaAs the data point to an increased mosaicity in the films, which seems to be independent from the indium content. This mosaicity might also contribute to the FWHM of the (004)-diffraction peak, so the dislocation densities given in Fig. 4 a) might have a constant offset and have to be seen as upper boundaries. Fig. 4 f) corresponds to a typical dark field TEM image of an $In_{0.17}Ga_{0.83}As$ film. Dislocations and a high density of twins were observed in the $In_{0.17}Ga_{0.83}As$ on graphene, supporting the findings from the HRXRD measurements. We also analyzed the surface morphology of the samples and provide atomic-force-microscopy (AFM) and scanning-electron-microscopy (SEM) images in the supplemental material (see Fig. S2-S3). The SEM image in Fig. S2 shows exemplarily a 200 nm thick $In_{0.30}Ga_{0.70}As$ film with some surface defects which might be introduced by the graphene film or during sample preparation. In addition, AFM images in Fig. S3 reveal a similar surface roughness of $In_xGa_{1-x}As$ films grown on graphene covered GaAs, with slightly higher RMS-roughness of films grown on graphene. In summary, the films on graphene exhibit more crystal defects than the corresponding films grown on bare GaAs.

We think, the stronger film relaxation together with a constant dislocation density independent of the indium concentration for layers grown on graphene point to a different strain relaxation compared to growth on bare GaAs. In [14], a slip of the entire film over the graphene for lattice mismatched layers grown on graphene to relax the lattice mismatch has been proposed and the energy required for a film slip of a mismatched film on a graphene covered substrate was calculated. This slip-energy is smaller compared to the energy required for the formation of dislocations in the film [14]. However, this mechanism results in a reduced dislocation density, whereas we observe an increased dislocation density. It seems that in our case the graphene makes the formation of dislocations easier compared to growth on bare GaAs. One reason might be that the transfer graphene layer exhibits pinholes or surface features where defects are introduced. Here, an optimized preparation of the graphene layer might improve the film quality. We also speculate that the graphene-induced changes in the growth mode, i.e., the island growth with subsequent coalescence, which is not considered in the modelling done in [14], might be relevant. Maybe the individual islands perform a slip over the graphene and relax in this way. However, the coalescence of the islands in the initial stage of growth introduces defects like stacking faults in the $In_xGa_{1-x}As$ films. We showed first investigations of remote $In_xGa_{1-x}As$ heteroepitaxy on graphene covered GaAs substrates and despite large progress in the substrate preparation, the $In_xGa_{1-x}As$ nucleation and the subsequent overgrowth, the material quality is still worse than growth on bare GaAs substrates. Careful optimization of the nucleation process and more detailed investigations of the island

coalescence should be considered in future investigations and might be able to improve the material quality so that it is sufficient for applications in optoelectronic devices.

4. Conclusion

In summary, we reported for the first time on the remote heteroepitaxy of $\mathrm{In_xGa_{1-x}As}$ layer on transfer graphene covered GaAs by solid source MBE. Commercially available transfer graphene was wet transferred to the GaAs substrates. XPS and Raman measurements reveal that a short plasma cleaning followed by UHV annealing removes the oxide layer in between GaAs and graphene while keeping the graphene mostly intact. We show that $\mathrm{In_xGa_{1-x}As}$ layer growth must be initialized by a thin nucleation layer growth at low temperatures and growth of thicker layers by a two-step process was performed. The single crystalline $\mathrm{In_xGa_{1-x}As}$ layer phase reveals successful transfer of the substrate crystal orientation to the layer. HRXRD and Raman spectroscopy reveal different strain relaxation in this mismatched system: A larger and significantly more isotropic relaxation is observed for layers grown on graphene. In contrast to growth on bare GaAs, layers grown on graphene exhibit no layer tilt and a constant dislocation density independent of the layer's indium concentration. For low indium concentrations, the defect density for the growth on graphene is higher than for growth on bare GaAs.

ACKNOWLEDGMENT

The authors like to acknowledge financial support by the Deutsche Forschungsgemeinschaft (DFG, German Research Foundation), Projektnummer 231447078-TRR 142 (via project A06),

REFERENCES

[1] T. Kujofsa, J. E. Ayers, *Journal of Electronic materials* **45**, 2831–2836 (2016). https://doi.org/10.1007/s11664-016-4377-9.
[2] R. Kumar, A. Bag, P. Mukhopadhyay, S. Das, D. Biswas, *Applied Surface Science* **357**, 922–930 (2015). https://doi.org/10.1016/j.apsusc.2015.09.145.
[3] K. Vanhollebeke, I. Moerman, P. Van Daele, P. Demeester, *Progress in Crystal Growth and Characterization of Materials* **41**, 1–55 (2000). https://doi.org/10.1016/S0960-8974(00)00045-0.
[4] Y. Alaskar, et al., *Advanced Functional Materials* **24**, 6629–6638 (2014). https://doi.org/10.1002/adfm.201400960.
[5] Y. Alaskar, et al., *Journal of Crystal Growth* **425**, 268–273 (2015). https://doi.org/10.1016/j.jcrysgro.2015.02.003.
[6] J. Kim, et al., *Nature communications* **5**, 4836 (2014). https://doi.org/10.1038/ncomms5836.
[7] A. Koma, *Thin Solid Films* **216**, 72–76 (1992). https://doi.org/10.1016/0040-6090(92)90872-9.
[8] J. Yu, et al., *Advanced Materials* **32**, 1903407 (2019). https://doi.org/10.1002/adma.201903407.
[9] K. Qiao, et al., *Nano Letters* **21**, 4013–4020 (2021). https://doi.org/10.1021/acs.nanolett.1c00673.
[10] H. Kim, et al., *ACS Nano* **15**, 10587–10596 (2021). https://doi.org/10.1021/acsnano.1c03296.

[11] Y. Kim, et al., *Nature* **544**, 340–343 (2017). https://doi.org/10.1038/nature22053.
[12] W. Kong, et al., *Nature Materials* **17**, 999-1004 (2018). https://doi.org/10.1038/s41563-018-0176-4.
[13] H. Kum, et al., *Nature Electronics* **2**, 439-450 (2019). https://doi.org/10.1038/s41928-019-0314-2.
[14] S.-H. Bae, et al., *Nature Nanotechnology* **15,** 272-276 (2020). https://doi.org/10.1038/s41565-020-0633-5.
[15] K. Badokas, et al., *Journal of Physics D: Applied Physics* **54**, 205103 (2021). https://doi.org/10.1088/1361-6463/abe500.
[16] S.-H. Bae, et al., *Nature Materials* **18**, 550–560 (2019). https://doi.org/10.1038/s41563-019-0335-2.
[17] D. Ferrah, et al., *ACS Applied Nano Materials* **2**, 1356-1366 (2019). https://doi.org/10.1021/acsanm.8b02249.
[18] B. Zhuang, S. Li, S. Li, J. Yin, *Carbon* **173**, 609-636, (2021). https://doi.org/10.1016/j.carbon.2020.11.047.
[19] C. Cunge, et al., *Journal of Applied Physics* **118** 123302 (2015). https://doi.org/10.1063/1.4931370.
[20] R. People, J. C. Bean, *Applied Physics Letters* **47**, 322-324 (1985). https://doi.org/10.1063/1.96206.
[21] B. Yarlagadda, et al., *Applied Physics Letters* **92**, 202103 (2008). https://doi.org/10.1063/1.2936078.
[22] M. Fatemi, J. Chaudhuri, J. Mittereder, A. Christou, *Journal of Applied Physics* **73**, 1154-1160 (1993). https://doi.org/10.1063/1.353282.
[23] R. Chierchia et al., *Journal of Applied Physics* **93**, 8918-8925 (2003). https://doi.org/10.1063/1.1571217